Molecular recognition and controlled release in drug delivery systems based on nanostructured lipid surfactants

2006 J. Phys.: Condens. Matter 18 S2203

(http://iopscience.iop.org/0953-8984/18/33/S35)

INSTITUTE OF PHYSICS PUBLISHING JOURNAL OF PHYSICS: CONDENSED MATTER

J. Phys.: Condens. Matter **18** (2006) S2203–S2220 doi:10.1088/0953-8984/18/33/S35

Molecular recognition and controlled release in drug delivery systems based on nanostructured lipid surfactants

R Angius[1], S Murgia[1], D Berti[2], P Baglioni[2] and M Monduzzi[1]

[1] Department Scienze Chimiche, CGSI University of Cagliari, S.S. 554 Bivio, Sestu 09042, Monserrato (CA), Italy
[2] Department Chimica, CSGI University of Florence, Via della Lastruccia 3, 50019 Sesto, Fiorentino (FI), Italy

E-mail: monduzzi@unica.it

Received 16 January 2006, in final form 27 June 2006
Published 4 August 2006
Online at stacks.iop.org/JPhysCM/18/S2203

Abstract

Several monoolein/water (MO/W) based liquid crystalline (LC) nanostructured mesophases have been revisited in view of the new trends of modern drug delivery formulations. The shape and amphiphilic character of the investigated lipid molecules address the preferential polar–apolar interfacial curvature and the delicate interplay of different intermolecular forces that drive self-assembly and thermodynamic stability of the nanostructures.

Here some preliminary results related to the release of the antiviral drug 1-amine-adamantane hydrochloride, solubilized in the aqueous domain of bicontinuous cubic and reverse hexagonal LC phases, suggest these MO based LC phases as possible nano-depot systems for long term controlled release. Drug release was followed by conductivity measurements during a period of ten days.

An effective and targeted drug delivery often requires a specific molecular recognition. With this aim, the possibility to entrap suitable molecules such as lauroylcholine (LCh, a cationic surfactant having a peptide-like polar head that can 'recognize' membrane proteins) and adenosine monophosphate disodium salt (NaAMP, an electrolyte that can 'recognize' purine receptors) has been tested. The addition of LCh to MO/W cubic gyroid (C_G) LC phase causes a cubic–lamellar phase transition. The addition of NaAMP still allows the formation of the C_G nanostructure. In the presence of both NaAMP and LCh again a C_G LC phase forms. The bicontinuous C_G LC phases have been characterized by NMR and SAXS.

1. Introduction

In recent developments surfactant and colloidal science has become the basis for bioscience and nanotechnology [1, 2]. The knowledge of surfactant self-assembly and the awareness of the interplay of hydrophobic–hydrophilic intermolecular interaction [3] play a crucial role in the projection of new systems for highly specific applications. In particular, making hierarchically ordered materials represents an important challenge to engineer intelligent biomaterials for bio-nanotechnological applications such as biosensors and drug delivery. Focusing the attention on drug delivery systems [4], the advances in drug discovery have been huge and would have been unpredictable 20 years ago. However, the high specificity, in terms of efficacy, obtained in drug production has not been accompanied by a specific targeting of the delivery systems: substantially efficacious drugs are available, pharmacologists know suitable drugs to attach the disease but the drug cannot be often delivered to the most suitable receptors, specifically. The acceleration in the discovery of new therapies based on chemical, biological, genetic and radiological moieties has brought an increasing demand for delivery systems capable of protecting, transporting and selectively releasing the therapeutic agents to the desired receptor site. In many cases there are physical barriers that prevent the drug from reaching the receptor. This is the case of the blood–brain barrier that protects neuroreceptors but at the same time does not permit the drug to go across.

The majority of drug delivery systems belong to the colloidal domain. They are solid–solid, solid–liquid, and liquid–liquid dispersions having, in most cases, a relatively long-term kinetic stability. Surface properties and interfacial interactions with the biological environments are crucial to determine the bioadhesion and then the release performance of the drug. Various steps and parameters involved in the drug delivery should be controlled [5, 6]: first the bioavailability (that is, the amount of therapeutic agent really available for the therapeutic action), the time dependent biodistribution at the specific receptor sites, then the pharmacokinetic and pharmacodynamic parameters which affect the therapeutic effectiveness, and finally the circulation lifetime and the immune response from phagocytic cells. These steps and parameters are controlled by intermolecular interactions due to surface charges, steric stabilization, phase behaviour, particle size, and hydrophilic–hydrophobic surface coating [7].

Among the crucial factors that are involved in modern drug delivery molecular recognition to address the drug to specific receptors and protection of the therapeutic agent from macrophages and immune response are of utmost importance. However, the most difficult challenge is the controlled drug release at very long term (months) for patients with low compliance. With this aim, the new trends are related to the development of nano-sized depot systems.

Substantially, most of the innovative drug delivery formulations are obtained exploiting nanoscience and nanotechnology advances. The biologically active nanoparticles may be of different types depending on the target. They include microsphere hydrogels (0.5–20 μm) based on polysaccharides [8], emulsions and microemulsions [9], liposomes [10], micelles [11], lipid nanoparticles such as cubosome®[3] and hexosomes® (see footnote 3) [12–18]. Actually, a variety of materials, from carbon nanotubes to polylactide nanoparticles, have been suggested to fulfil the new demands of drug delivery performance.

Here the highlight is on lipid based systems since they are generally friendly towards biological membranes. In this context, in the past decade, it has been assessed that molecular recognition can address the specific interaction [19–25] required by a targeted delivery.

[3] ®Camurus Lipid Research Registered Trademark, Lund (Sweden).

In general, molecular recognition can be attained through different molecular mechanisms driven by electrostatic and H-bonding mainly. They may involve protein–substrate interactions, lipid diffusion, and structural changes in the membrane [20]. Modified nucleosides and nucleotides have been the main choice with this aim, while liposome architectures have been the most used lipid nanostructures as interacting carrier for the recognition studies. Indeed, a variety of nucleoside based agonists and antagonists of the purine and pyrimidine receptors have been synthesized [26]. Recently, it has also been recognized that carbohydrate mediated liposomal interaction may improve the adhesion to the target cell [27]. Carbohydrate ligands may be related to glycoproteins, glycolipids, viral proteins, and lipopolysaccharides that can play the molecular recognition role themselves or reinforce it. Thus nowadays intelligent biomaterials would combine molecular recognition with drug release. Modelling the supramolecular arrangement along with the functionality in terms of molecular recognition is an important target of biomedical and pharmaceutical research, and has become a major challenge of soft matter science.

2. The packing parameter concept

It is well assessed that drug delivery systems based on surface active molecules possess the capability to implement bioadhesion due to the self-assembly properties. These, in turns, are strongly influenced by the shape of the polar–apolar interface and thus by the geometric features of the surfactant molecules.

The aggregate supramolecular architecture can be described by the geometry of the interface dividing the hydrophobic and hydrophilic domains [28]. This interface is characterized by two distinct contributions: the interfacial curvatures, related to the local geometry, and the interfacial topology, that describes the global geometry in terms of the degree of interfacial connectivity. As firstly defined by Ninham *et al* [29–31] the local constraint upon the curvatures of the interface is given by the packing parameter of the surfactant, v/al (v is the hydrophobic chain volume, a is the head group area and l is the chain length, taken as 80% of the fully extended chain).

The surfactant packing parameter is very useful to predict which phases can be preferentially formed by a given surfactant since it connects the molecular properties with the favoured curvatures of the aggregate interface. Actually, the v/al parameter is related to the mean and the Gaussian curvatures, respectively H and K, on the basis of the following equation derived from differential geometry [28]:

$$v/al = 1 + Hl + Kl^2/3. \tag{1}$$

Generally, if $v/al < 1$ surfactants form spherical or cylindrical micelles, when $v/al \approx 1$ the lamellar aggregates are favoured, and if $v/al > 1$ aggregates with reverse curvature form [31]. In real systems, effective packing parameters should be considered. The v/al ratio can change as a consequence of temperature variations, oil or water addition or the introduction of a new component. For instance, the surfactant volume chain increases if a highly penetrating oil is added, and the area of the polar head changes by adding a salt or changing the temperature (different hydration strength). Hence the composition can change v/al, and then microstructure and also interfacial topology can be modified. Alternatively, structure modifications can occur as a result of curvatures' variations, in equation (1), which, however, do not alter v/al [28].

Figure 1 shows the typical shapes of the nanostructures, micelles and liquid crystals (LCs), that can form as a function of the packing parameter v/al or, alternatively, the mean interfacial curvature H. The curvature H is assumed to be positive ($H > 0$) for the oil-in-water (o/w)

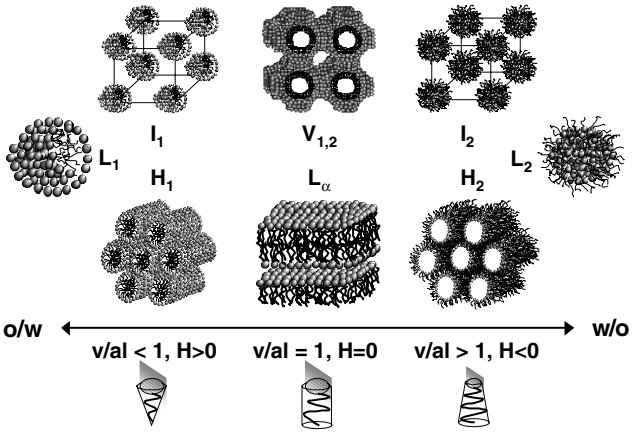

Figure 1. Schematic representation of the most common supramolecular structures formed by surfactants as a function of both the molecular shape (packing parameter—see the text) and the interfacial mean curvature (H). $L_{1,2}$, micellar phase; $H_{1,2}$, hexagonal phase; $I_{1,2}$, discrete cubic phase; $V_{1,2}$, bicontinuous cubic phase; L_α, lamellar phase. Subscripts '1' and '2' indicate normal (o/w) and reverse (w/o) phases, respectively.

microstructures and negative ($H < 0$) for the water-in-oil (w/o) microstructures. Lamellar and bicontinuous cubic LC phases have a mean interfacial curvature $H = 0$, by definition.

Here, it should be reminded that, in the case of some lipid molecules, the bicontinuous cubic phases are constituted by curved non-intersecting bilayers organized to form two disjoint continuous water channels [28]. If a plane is placed in the gap between the end groups of the lipid bilayer of the cubic phase, the surface obtained can be described by an *infinite periodic minimal surface* (IPMS) [32, 33]. The curvature of any surface is given by the two principal curvatures, k_1 and k_2. The mean curvature $H = (k_1 + k_2)/2$ at any point of a minimal surface is zero by definition. The packing parameter, v/al, for a lipid in such a curved bilayer is close to or slightly larger than unity and can be related (see equation (1)) to the Gaussian curvature $K = k_1 k_2$ of the IPMS [34]. Three types of IPMS, describing different cubic space groups, are important in lipid systems [32, 33]: the diamond (C_D) type (primitive lattice $Pn3m$), the gyroid (C_G) type (body-centred lattice $Ia3d$), and the primitive (C_P) type (body-centred lattice $Im3m$).

3. Monoolein based formulations

At the present state of art, lipid based formulations (liposomes, emulsions and microemulsions, liquid crystals) represent powerful and stimulating nanostructured biomaterials which can be easily modulated to tune drug delivery structural properties and controlled drug release performance.

Since some pioneering works [33, 35–40] where the monoolein (MO) phase behaviour in water was clarified and found to mimic several membrane features, many investigations have appeared on the possible use of MO based systems for drug delivery.

MO, used as an emulsifier and food additive since 1950, more recently has received great attention for applications in the pharmaceutical area as reported by some reviews [41–43]. The existence of two types of bicontinuous cubic phases, namely the gyroid C_G ($Ia3d$ space group) and the diamond C_D ($Pn3m$ space group), is well known and demonstrated for the MO/W system [38, 39]. A lamellar (L_α) LC phase forms at low water content, whereas the C_G phase

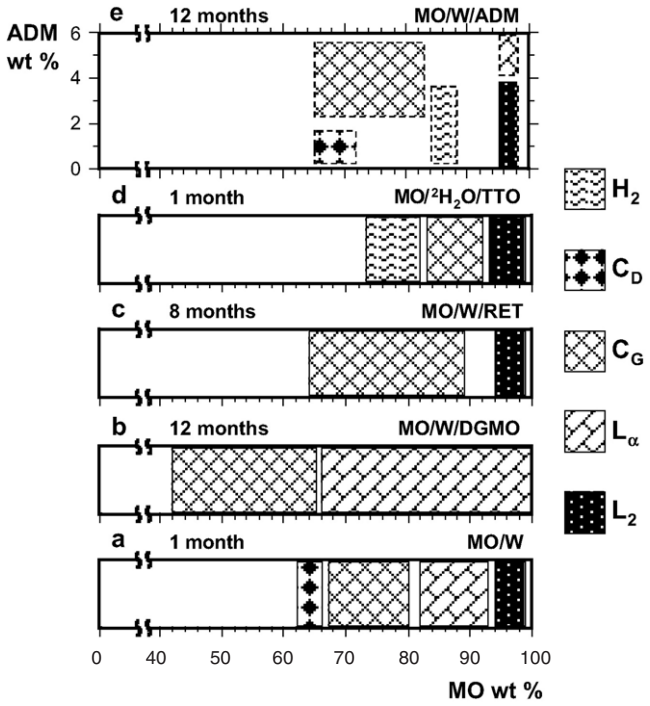

Figure 2. Modifications, at 25 °C, of the MO/W [39] binary phase diagram (a) induced by the presence of various additives: (b) 15 wt% of DGMO [47]; (c) 1 wt% RET [48]; (d) 5 wt% TTO [51]; (e) 1–6 wt% ADM [52]. The phase diagrams are obtained at different samples storage times (1, 12, 8, 1, and 12 months, respectively), and data are taken from the given references. For acronyms see the text and figure 1 caption.

evolves towards a reverse hexagonal (H_2) LC phase at high temperature. Figure 2(a) (data from [39]) shows the phase diagram of MO/W at 25 °C, where a small region of liquid L_2 phase that forms in the presence of a minimal amount of water (1–6 wt%) is reported.

MO based drug delivery systems of various types for topical, oral, and periodontal use have been developed, as well as colloidal carrier systems to control the release of drugs [41, 43].

In many applications, in particular for parenteral drug delivery, MO based cubic and reverse hexagonal liquid crystalline phase systems were dispersed in colloidal nanoparticles, cubosomes, and hexosomes, stabilized by a nonionic triblock polymer (Poloxamer 407) as stabilizing agent [12–14]. Whereas cryo-TEM [13] and AFM [15] have shown that the fracture of the liquid crystalline phases produces nanoparticles of cubic and hexagonal shapes, NMR techniques have demonstrated that the intrinsic microstructure of these cubic and hexagonal nanoparticles is not altered by the dispersion process [16]. Figure 3 shows the cryo-TEM (courtesy of Kåre Larsson) and AFM microscopy images obtained for these cubic and hexagonal nanoparticles dispersed in water. To improve bioavailability, cubosomes based on higher amounts of phospholipids along with polyethyleneglycol have been recently reported [18].

Recently, other easier-to-deal-with formulations have been developed to overcome the limitations imposed by the use of LC phases for drug delivery purposes. Creamy emulsions endowed with very long shelf life were obtained by adding to MO/W systems lecithin (LCT) or di-glycerol-monooleate (DGMO), and triolein (glycerol-trioleate GTO) as oil [44, 45]. In

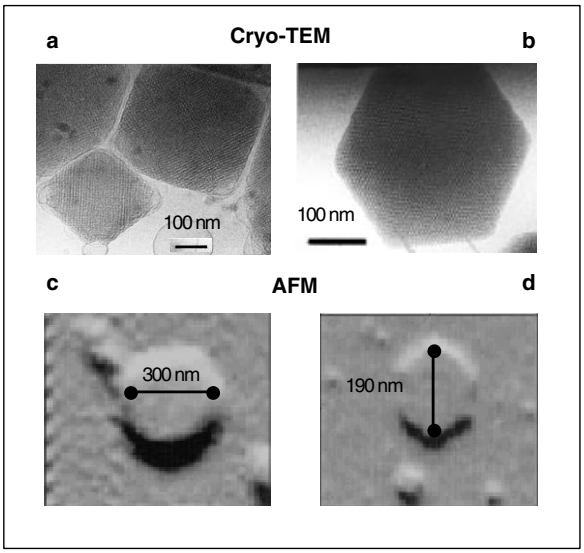

Figure 3. Images from cryo-TEM, (a) cubosome and (b) hexosome (courtesy of Kåre Larsson), and AFM, (c) cubosome and (d) hexosome, at 25 °C.

particular, it was ascertained that the prolonged kinetic stability of the water droplets in the emulsions is mainly due to a dispersing medium constituted by a mixture of reverse hexagonal (H_2) and lamellar (L_α) LC phases. In these systems hydrophilic substances may be easily dispersed. Figure 4 shows the partial diagrams of the emulsion regions, redrawn from [45], formed by MO/W/GTO systems. It is worth noticing that the increase of GTO content, at low water content, produces clear and thermodynamically stable w/o microemulsions (L_2 phases), where also hydrophobic drugs may be easily solubilized.

Many investigations have focused on the modifications of MO/W system phase behaviour in the presence of other components. The modifications induced in the MO/W system strongly depend on polarity, shape, and concentration of the additive [46–51]. The nanostructures of these systems were investigated through optical microscopy and SAXS for the qualitative characterization, and through NMR relaxation and self-diffusion techniques for the dynamic aspects. As an example, figures 2(b)–(e) show the modifications of the MO/W phase diagram at 25 °C due to the addition of, respectively, di-glycerol-monooleate (DGMO, 15 wt%, data from [47]), retinol (RET, 1 wt%, data from [48]), 1-aminoadamantane hydrochloride (ADM, 1–6 wt%, data from [52]), and *Melaleuca alternifolia* essential oil (tea tree oil—TTO, 5 wt%, systems examined in ^2H_2O, data from [51]).

It should be emphasized that the packing parameter $v/al = 1.06$ (where $v = 630$ Å^3, $a = 35$ Å^2, and $l = 17$ Å) of MO is crucial to determine the possibility of incorporating both hydrophilic and hydrophobic species [53]. Indeed, the interfacial curvatures related to packing parameters around unity allow microstructural fluctuations and transitions in agreement with the observation that the topology of the interface can change rather quickly upon small variation of the hydrophobic volume fraction [54]. A regular swelling is generally observed in the case of L_α and C_G LC phases. Alternatively, phase transitions may occur, but other thermodynamically stable LC nanostructures often form. It is not always clear if the effective v/al changes during the observed transitions. Certainly, the process involves a variation of the Gaussian curvature K from the negative values of a continuous bilayer in the C_G and C_D LC phases (mean curvature

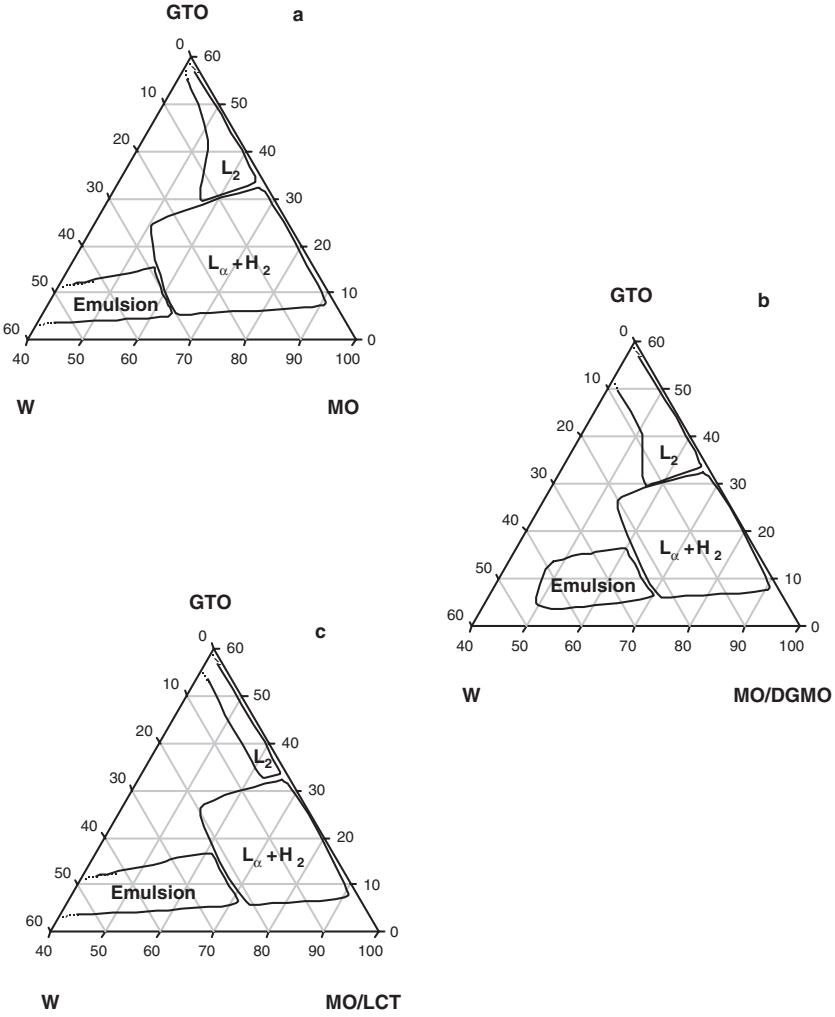

Figure 4. Partial ternary and pseudo-ternary diagrams, at 25 °C, of systems (a) MO/W/GTO and (b) MO-DGMO/W/GTO where MO/DGMO = 85/15, (c) MO-LCT/W/GTO where MO/LCT = 95/5. LC phase acronyms as in figure 1.

$H = 0$) to the positive values of the L_2 LC phases through a $\langle K \rangle = 0$, a value typical of architectures having one flat surface such as H_2 (cylinder) and L_α phases.

4. Controlled release experiments

Samples containing various amounts of ADM and water may form different LC structures as shown in figure 2(d). Some of them were also investigated for the release performance. The focus was on the assessment of both the availability of the drug and the structural evolution of the LC matrix due to the release. The experiments were carried out posing the LC phases in contact with different amounts of water. Release was monitored by measuring the conductivity increase in the water phase for 3–10 days.

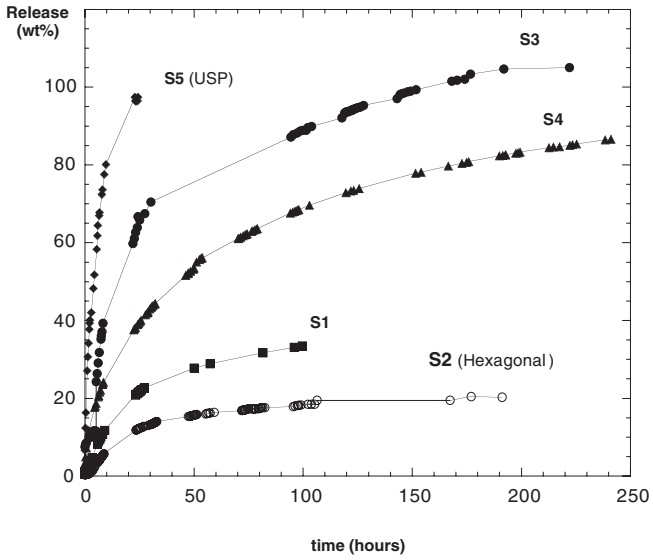

Figure 5. Release experiments of ADM in water from different MO LC phases at 25 °C, except for sample S1, where $T = 20$ °C was used.

Table 1. Samples used for the release experiments at 25 °C (except S1).

Sample	Composition MO/W/ADM (wt%)	LC phase	Ageing	Release[a] (g ml^{-1})
S1	62.9/34.1/3.0	V_2	10 d.	2.1/3 (20 °C)
S2	79.1/17.4/3.5	H_2	12 m.	2.2/3
S3	62.9/34.1/3.0	V_2	9 m.	2.0/25
S4	78.3/18.2/3.5	$V_2 + H_2$	9 m.	3.7/30[b]
S5	79.0/18.0/3.0	V_2	3 m.	0.119/20[c]

[a] Release conditions: grams of sample per volume of water used in the release experiment.
[b] Stirring used during the experiment; H_2 LC after the release.
[c] A USP-type method (see the appendix) was used.

Table 1 shows some data for these samples, whereas figure 5 shows the release profiles of ADM, referred to the total amount of the drug initially present in the LC phase for each system.

Before discussing the results it should be noticed that, compared to data previously reported [48], samples with water content around 17–20 wt% and ADM content around 3–3.5 wt% underwent C_G-to-H_2 phase transitions upon aging more than 8 months (see S2 and S4 samples). This can be ascribed to free oleic acid (OA) that forms as a consequence of MO hydrolysis. OA, being located at the polar–apolar interface with a much smaller polar head than MO, determines a preferential mean negative curvature (see figure 1). The instability of these LC phases upon long storage prevented a really accurate investigation on the release performance. However, it was possible to ascertain, at a qualitative level, that several parameters affect the release performance. With increasing the volume of water for the release, 100 wt% of the drug is recovered in 10 days for sample S3 and in 30 h for sample S5 where a USP-type method and a very high volume of water were used. The presence of H_2 LC phase decreases the amount of released drug as in the case of samples S2 and S4: in the latter case, stirring the solution where drug is released and increasing the volume for the release seem to affect the release performance significantly.

As to the LC phase stability, sample S1, that before the release experiment was a C_G phase ($Ia3d$ space group with $\alpha = 120$ Å), became a turbid C_D phase ($Pn3m$ space group with $\alpha = 106$ Å) after 100 h of release. This transition corresponds to a significant decrease of the effective lipid volume fraction Φ_l from 0.786 ($Ia3d$ phase) to 0.586 ($Pn3m$ phase) as can be estimated from the relation [55]

$$\Phi_l = 2A_0\left(\frac{l}{\alpha}\right) + \frac{4\pi\chi}{3}\left(\frac{l}{\alpha}\right)^3 \tag{2}$$

where A_0 and χ are the surface area and Euler characteristic of the IPMS geometries ($Ia3d$, $A_0 = 3.091$, $\chi = -8$; $Pn3m$, $A_0 = 1.919$, $\chi = -2$) [28, 32, 55, 56], α is the lattice parameter from SAXS and $l \approx 17$ Å is the MO chain length as obtained from the relation l (Å) $= 18\exp(-0.0019\,T)$, where T is temperature in °C [55]. In other words, the variation of the cubic arrangement and of the spacing α may suggest a decrease of the Gaussian curvature K (from 0.0011 to 0.0002) of the MO bilayer according to the relation [28]

$$\alpha = \frac{(2\pi\chi)^{1/3}}{(H)^{1/3}\langle K\rangle^{1/2}} \tag{3}$$

where H is the homogeneity index ($Ia3d$, 0.7665; $Pn3m$, 0.7498). It should be admitted that all these figures are mere speculations. This experiment was performed at 20 °C. Because of turbidity formation (due to coexistence of the C_D phase with water excess) the experiment was interrupted after three days, and only about 30 wt% of ADM was recovered. Moreover, it should be mentioned that, compared to sample S3 (the same composition as S1), a very small volume of water was used. However, comparing S1 and S3 initial release performance, the effect of temperature is significant. The case of sample S4 is also questionable. Sample S4, that after 9 months from preparation was a mixture of C_G and H_2 LC, became a single H_2 phase after a 10 days release experiment. Because of the contact with a relatively large amount of water a swelling of the C_G phase to C_D LC phase would have been predicted. In fact, a H_2 phase forms, very likely as a result of ADM release from the water channels and concomitant OA effects.

These are preliminary results only, since real *in vitro* release experiments would involve several additional parameters and different conditions, particularly a physiological temperature around 37 °C. Nevertheless, these data suggest the MO based LC bicontinuous cubic and reverse hexagonal phases as suitable drug delivery systems. Moreover, in consideration of the release performance, these systems might be used as depot carriers provided that a final delivery formulation is developed. Therefore other more targeted investigations are in progress.

5. Molecular recognition

To our knowledge, only a few investigations have reported inclusion of molecules which might be of interest for molecular recognition (glucose, creatinine, cytochrome-c, cyclic-AMP and its dibutyryl analogue) [57–59]. In the case of cyclic-AMP it was shown that due to its high hydrophilicity no specific binding to the polar–apolar interface of the C_D LC phase occurs, whereas the dibutyryl analogue inserts into the bilayer, thus inducing a C_D–C_G phase transition.

Here AMP disodium salt (NaAMP) and lauroylcholine chloride (LCh) are considered as additives to promote molecular recognition. Figure 6 shows a picture of these molecules along with MO to point out the shape.

NaAMP, exactly like cyclic-AMP, is expected to solubilize in the water domain. LCh is likely to locate at the polar–apolar interface with the choline chloride group within the water domain. A sample having an MO/W $\approx 7/3 = 2.33$ weight ratio with a C_G ($Ia3d$ space

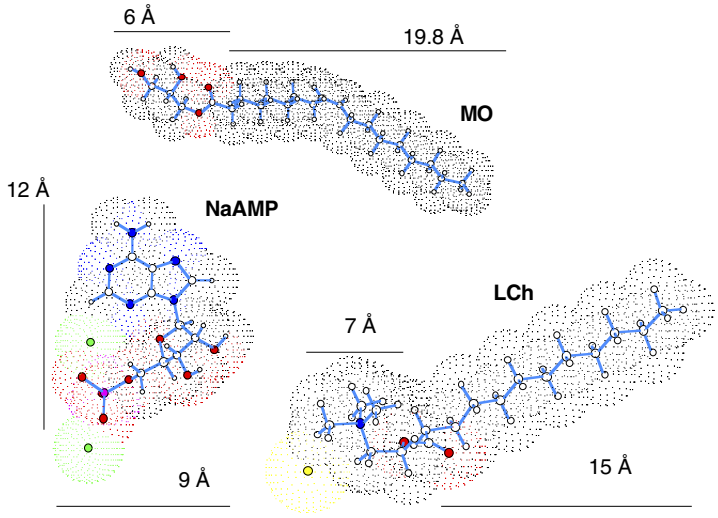

Figure 6. Space filling picture of MO, LCh, and NaAMP molecules.
(This figure is in colour only in the electronic version)

group) microstructure was chosen for testing the solubilization of the additives. Adding 3 wt% of LCh induces a C_G–L_α phase transition, whereas the addition of about 2 wt% of NaAMP still allows the formation of the C_G phase. When both the additives NaAMP and LCh are added in the molar ratio NaAMP/LCh $= 1/2$, the cubic phase is re-established due to the increase of the polar volume fraction. Indeed Na^+, AMP^{2-}, and Cl^- ions and the choline group, that is positively charged, are located in the water domain. Two MO/W/NaAMP and MO/W/LCh/NaAMP cubic samples were analysed for microstructure and dynamic features by SAXS and NMR measurements.

Figure 7 shows the typical $Ia3d$ patterns obtained for the two samples. Table 2 summarizes the SAXS data, and tables 3 and 4 the NMR results.

Although there are some weak and very weak reflections, SAXS patterns indicate the $Ia3d$ lattice spacing, typical of the bicontinuous cubic phase C_G, clearly. On the basis of equation (2) it can be suggested that the increase of spacing is related to a decrease of the effective lipid volume fraction from $\Phi_l = 0.76$ in the three-component to $\Phi_l = 0.72$ in the four-component system. Recalling that the IPMS is defined as the midplane surface dividing the bilayers of the bicontinuous cubic phase, the average radius of the IPMS is the sum of the water channel radius r_w and, in our case, of the MO chain length ($l \approx 17$ Å).

It has been shown that the cross sectional area $A(x)$ estimated on a surface parallel to and at a distance x from the minimal surface is related to the lattice parameter according to the relation [32, 55]

$$A_0\alpha^2 + 2\pi\chi x^2 = A(x) \tag{4}$$

where, introducing the pertinent values for the $Ia3d$ IPMS and considering that $A(x) = 0$ at the centre of the water channel, the water channel radius r_w can be evaluated from the spacing α according to

$$r_w = \left(\frac{3.091}{16\pi}\right)^{1/2}\alpha - 17 \tag{5}$$

after subtracting the contribution of the MO chain length of 17 Å. Introducing in this

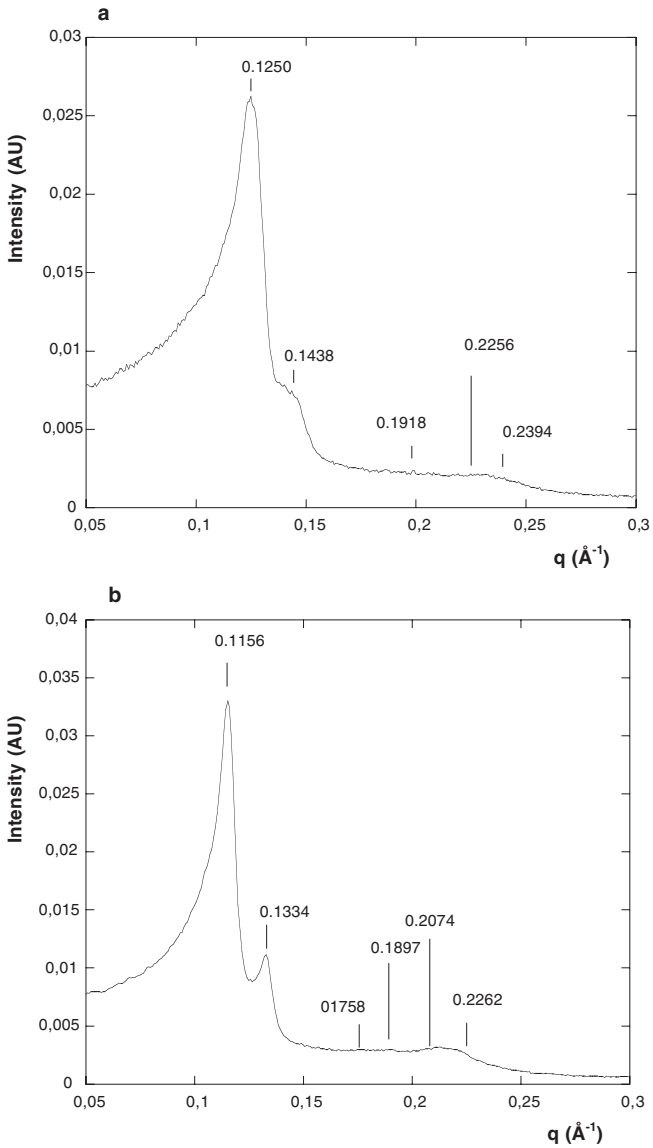

Figure 7. SAXS patterns at 25 °C of the two *Ia3d* cubic samples: (a) MO/W/NaAMP; (b) MO/W/LCh/NaAMP.

equation (5) the lattice parameters obtained by SAXS experiments, a water channel radius of 13.6 and 16.0 Å can be estimated for the MO/W/NaAMP and MO/W/LCh/NaAMP cubic samples, respectively. These figures agree with the calculated decrease of Φ_l values. According to [55], these figures are estimates and other models may be used to evaluate water channel radius. It should be mentioned that no significant differences were determined in the case of the C_D LC phases of the MO/W system examined by the same authors [55]. In this context it must also be mentioned that several authors have investigated MO/W cubic phases by SAXS measurements. Among the results reported in [39, 47, 55], slightly different spacing values are

Table 2. SAXS data of the two cubic MO systems.

d_{hkl} (Å)[a]	$(h^2+k^2+l^2)$	α (Å)[b]
MO/W/NaAMP = 68.45/29.45/2.10 (see figure 7(a))		
50.26 (s)	6	123.12
43.69 (s)	8	123.58
32.76 (w)	14	122.57
(n.d.)	16	—
27.85 (vw)	20	124.55
26.24 (vw)	22	123.10
Ia3d space group (C_G)—spacing $\alpha = 123.4 \pm 0.7$ Å		
MO/W/LCh/NaAMP = 66.23/28.42/3.35/2.00 (see figure 7(b))		
54.35 (s)	6	133.14
47.10 (s)	8	133.22
35.74 (w)	14	133.73
33.12 (w)	16	132.49
30.30 (vw)	20	135.48
27.78 (vw)	22	130.29
Ia3d space group (C_G)—spacing $\alpha = 133.1 \pm 0.5$ Å		

[a] $d_{hkl} = 2\pi/q$; s = strong; w = weak; vw = very weak.
[b] Lattice parameter $\alpha = d_{hkl} \times (h^2+k^2+l^2)^{1/2}$.

Table 3. NMR relaxation and diffusion data.

NMR nucleus	T_1 (s)	T_2 (s)	D ($\times 10^{10}$ m^2 s^{-1})
NaAMP 0.183 M in W			
NaAMP (^{31}P)	4.63 ± 0.11	1.94 ± 0.05	6.3 ± 0.2
NaAMP (^{23}Na)	0.0324 ± 0.0003	0.0317 ± 0.0003	9.4 ± 0.2
MO/W/NaAMP = 68.45/29.45/2.10			
NaAMP (^{31}P)	2.22 ± 0.04	0.310 ± 0.006	0.31 ± 0.02
NaAMP (^{23}Na)	0.0147 ± 0.0002	0.0137 ± 0.0002	2.02 ± 0.03
MO (^{13}C)	See table 4	—	0.127 ± 0.005
W (^{1}H)	—	—	3.7 ± 0.2
MO/W/LCh/NaAMP = 66.23/28.42/3.35/2.00			
NaAMP (^{31}P)	1.65 ± 0.03	0.131 ± 0.003	0.29 ± 0.02
NaAMP (^{23}Na)	0.0156 ± 0.0002	0.0145 ± 0.0002	2.02 ± 0.03
LCh (^{13}C)	—	—	0.19 ± 0.02
MO (^{13}C)	See table 4	—	0.121 ± 0.003
W (^{1}H)	—	—	3.7 ± 0.2

obtained depending on the purity of MO. Moreover, in the mentioned works, the swelling of the C_G phase, according to IPMS topology and notations, highlights some discontinuities around the MO/W = 7/3 compositions at 25 °C.

Table 3 shows relaxation and diffusion NMR results obtained to characterize the interactions between the molecules inserted in the cubic LC phases. As a comparison, some data for NaAMP in water, at the same concentration (0.183 M, referred to water content) as in the LC phase, are also given.

Table 4. ^{13}C NMR spin–lattice relaxation times (T_1) and chemical shifts (δ) of some MO carbons (G notations indicate the polar head glycerol carbons).

MO carbons	δ (ppm)	T_1 (s) MO/W/NaAMP	T_1 (s) MO/W/LCh/NaAMP
G_1	65.32	0.300 ± 0.003	0.309 ± 0.003
G_2	70.02	0.479 ± 0.005	0.487 ± 0.005
G_3	63.07	0.325 ± 0.004	0.332 ± 0.004
C_1	174.10	3.40 ± 0.04	3.43 ± 0.04
C_2	33.99	0.392 ± 0.004	0.402 ± 0.004
C_3	25.06	0.436 ± 0.005	0.445 ± 0.006
C_9	129.60	0.539 ± 0.006	0.559 ± 0.006
C_{10}	129.73	0.601 ± 0.007	0.618 ± 0.008
C_{16}	32.19	0.948 ± 0.009	0.98 ± 0.01
C_{17}	22.87	1.35 ± 0.02	1.40 ± 0.03
C_{18}	14.10[a]	2.58 ± 0.03	2.68 ± 0.03

[a] Used as internal reference for chemical shifts.

NaAMP is expected to behave as an electrolyte in water, but it should be mentioned that it is known to give stacking self-assembly due to the π–π interactions of the adenine aromatic rings already above a 0.05 M concentration. ^{31}P and ^{23}Na NMR relaxation and self-diffusion data reveal that such behaviour is actually exhibited in water solution. ^{23}Na NMR relaxation demonstrates that Na^+ ions are almost free to move in water solution since $T_1 \approx T_2$. The decrease of the relaxation times compared to a NaBr solution (0.04 M) for which $T_1 \approx T_2 = 48$ ms may be partly due to the increase of viscosity induced by adenine stacking. A rotational correlation time of 1.1×10^{-11} s can be calculated. This value should be compared to that, not very different, of 7.34×10^{-12} s, measured in the NaBr solution. A slight increase of viscosity is also confirmed by a decrease of the water self-diffusion coefficient of about 8%. Adenine stacking phenomena are clearly confirmed by the significant differences between T_1 and T_2 measured for the phosphate group by ^{31}P NMR relaxation experiments. Extreme narrowing conditions do not apply because of the self-assembly.

The self-diffusion coefficients D measured for Na^+ ions and for the phosphate group by ^{23}Na and ^{31}P NMR self-diffusion experiments further assess these statements. Na^+ ions move rather freely in the water solution with a $D = 9.4 \times 10^{-10}$ m^2 s^{-1} that has to be again compared to a value of 1.06×10^{-9} m^2 s^{-1} in the 0.04 M NaBr solution. This latter value corresponds to the diffusion of the fully hydrated Na^+ ions. A slightly, but significantly, slower self-diffusion coefficient is determined for the AMP anionic species. Due to the stacking phenomena a more significant decrease of the ^{31}P NMR self-diffusion coefficient would have been expected. In fact it should be recalled that diffusion measurements are mainly determined by the fastest diffusion species. According to a two-site free–bound model (free AMP^{2-} and self-assembled AMP^{2-} molecules) where D_{free} and D_{bound} may differ by at least one order of magnitude,

$$D_{\text{obs}} = p_{\text{free}} D_{\text{free}} + p_{\text{bound}} D_{\text{bound}} \tag{6}$$

a small amount of free monomers is sufficient to increase significantly the observed self-diffusion coefficient D_{obs}, provided that fast exchange occurs on the NMR timescale (the observation time $\Delta - \delta/3$, used in the spin-echo experiments—see the appendix). The opposite trend usually happens in the case of relaxation measurements:

$$1/T_{\text{obs}} = p_{\text{free}} 1/T_{\text{free}} + p_{\text{bound}} 1/T_{\text{bound}} \tag{7}$$

since $(1/T)_{1,2\text{bound}} \gg (1/T)_{1,2\text{free}}$.

Turning the attention to the cubic LC phases it is worth noticing again the differences between T_1 and T_2 for the phosphate group, and particularly the decrease of one order of magnitude of T_2 in the three-component and even more in the four-component system. This result indicates an increased hindrance of the phosphate groups in the water channels of the bicontinuous cubic phase that increases further in the presence of LCh. The decrease of the spin–spin (T_2) relaxation times is often associated to binding interactions since, with increasing the rotational correlation time (slow motion regime), the frequency independent term $J(0)$ becomes more important than in the fast motion regime. The self-diffusion coefficients measured by ^{31}P NMR are also significant. The decrease of mobility amounts to more than one order of magnitude. It is worth noticing that ^{31}P NMR self-diffusion coefficients, although higher, are of the same order of magnitude as those measured for MO and LCh by ^{13}C NMR. Phosphate groups and carbon skeletons in the bilayer move together. ^{23}Na relaxation times in the two cubic LC phases halve but $T_1 \approx T_2 \approx$ 14–15 ms is still measured. This brings us to calculate rotational correlation times around $\tau_c = 2.4 \times 10^{-11}$ s for Na^+ hydrated ions in the two cubic phases. Despite the confinement of these ions into water conduits having 2.6–3.2 nm diameters, they still reorient freely in solution. It should be recalled that the extreme narrowing condition may hold up to about $\tau_c =$ 2–4 ns for ^{23}Na at the observed magnetic field strength (7 T). The absence of strong interactions between Na^+ ions and the other species is further suggested by the ^{23}Na NMR self-diffusion coefficients that amount to 2×10^{-10} m^2 s^{-1} in both cubic LC samples. Indeed, a self-diffusion coefficient about one-third of that measured in the bulk solution ($9.4/3 \approx 3.1$) for sodium ions and ($6.3/3 = 2.1$) for phosphate groups would have been expected for species allowed to move freely in one direction only. Here a slightly lower value is measured for Na^+ ions as a result of the obstruction produced by MO polar heads (LCh polar heads also in the four-component system) and AMP^{2-} anions. As already pointed out, the large decrease of the phosphate group self-diffusion coefficient confirms the occurrence of strong interactions between AMP^{2-} anions and the surrounding environment.

All these findings validate the NaAMP molecule as a molecular probe to investigate the interactions between the polar domain and the interface.

In MO based cubic (C_G) phases it has been observed that spacing increases with increasing water content [39, 47, 55], and, in parallel, water self-diffusion coefficients also increase [60]. This is reasonable, and well assessed, if MO only is considered. But this behaviour is not actually observed in the present work. The self-diffusion coefficients, measured by NMR, do not indicate specific differences between the two cubic samples. The solubilization of 2 wt% of NaAMP should increase the volume fraction of the polar domain. In the four-component system, there is less MO, and the expected contribution of the LCh alkyl chain must be less significant than that found in the MO/W/LCh system (3 wt% of LCh, added to an MO/W $= 7/3$ sample, promotes a cubic–lamellar phase transition). In the presence of both LCh and NaAMP, the LCh polar head, that is positively charged, is likely to interact with AMP^{2-} anions. This results in a decrease of the effective lipid volume fraction as calculated from equation (2). This, in turn, determines an increase of the water channel radius as calculated from equation (5), but no changes occur in the self-diffusion coefficients of the moieties located in the water domain. This may be the result of the molecular interactions between the AMP^{2-} and choline charged species as suggested by ^{31}P NMR relaxation data (particularly T_2). No changes occur in the MO bilayer skeleton either as demonstrated by ^{13}C NMR relaxation times reported in table 4. As previously observed [49], here it is again confirmed that solubilization of hydrophilic, hydrophobic, or surfactant moieties does not modify the intrinsic organization of the MO molecules in the bilayer.

In the present case the role of the surfactant LCh may be significant. LCh presence reinforces the interactions with NaAMP and concomitantly swells the C_G LC phase to higher

lattice spacing. This result agrees with the observations on the phase behaviour induced by sodium oleate, an anionic surfactant, in MO/W systems [61]. Also in this case an increase of spacing was determined for the C_G LC phase.

These are only preliminary results, but they clearly indicate significant interactions between LCh and NaAMP entrapped in MO LC phases, therefore further work is in progress to investigate phase diagrams, intermolecular interactions and release performance.

6. Conclusions

Here MO based formulations have been considered. As already emphasized by Larsson [37, 38] 20 years ago, monoglyceride based drug delivery formulations are very important, and probably their potentialities have not yet been fully exploited. Cubosome and hexosome nanoparticles as well as LC phases are not easy-to-deal-with systems, the nanoparticles being temperature sensible and not thermodynamically stable dispersed systems, whereas the LC phases, although thermodynamically stable, are difficult to manipulate and undergo phase transitions with time due to monoglyceride hydrolysis.

It has been found that 15 wt% of DGMO prevents phase transition due to hydrolysis for at least 2 years. Indeed, hydrolysis and consequent phase transitions caused several problems in the systems containing ADM. Nevertheless, it has been shown that a potential depot system might be realized provided that a final delivery formulation is projected.

Finally, MO based LC phases seem to be suitable nanocontainers for molecules having potentiality for molecular recognition.

Acknowledgments

MIUR-Prin 40% (Italy), and Consorzio Sistemi Grande Interfase (CSGI, Italy) are acknowledged for financial support. Kåre Larsson (Camurus, Lund, Sweden) is thanked for the unpublished cryo-TEM images.

Appendix

Materials. Monoolein (MO, 1-monooleoylglycerol, RYLO MG 90-glycerol monooleate; 98.1 wt% monoglyceride) was kindly provided by Danisco Ingredients, Brabrand, Denmark. The 1-amine-adamantane hydrochloride is an Acros Organic product (99% purity), lauroylcholine chloride (LCh) is from Sigma, and adenosine-5′-monophosphate disodium salt (NaAMP, purity $\geqslant$ 99.0%) is from Fluka BioChemika.

Distilled water (W), passed through a Milli-Q water purification system (Millipore), and deuterated water (D) from Fluka were used to prepare the samples.

Sample preparation. Samples were prepared by weighing the components into glass tubes ($\varnothing \approx 0.5$ cm) that were centrifuged, frozen for 12 h, and flame-sealed. They were homogenized by repeated cycles of heating at 30 °C and centrifuging back and forth at 3000 rpm at 25 °C. Samples used for the phase diagram characterization were stored at 25 °C in the dark for three weeks before any measurement was made. Conversely, samples containing NaAMP were analysed immediately after they appeared homogeneous by visual inspection (about one week after their preparation) and then stored at 5 °C to prevent mould formation.

Conductivity measurements. Conductivity measurements were performed using a microprocessor conductivity meter from WTW.

Release experiments. The release of ADM, from different liquid crystalline samples to an aqueous medium, was followed measuring the conductivity of ADM in water, within a

maximum period of ten days. Before starting the experiments, a calibration line of the drug conductivity in water at 20 and 25 °C, at different concentrations, was performed.

The release experiments were performed on samples of different ages, using different amounts of the liquid crystalline phases. Different volumes of water (see table 1) were placed over the liquid crystalline phase, just before inserting the conductivity cell. Stirring of sample S4 was performed by fixing the whole apparatus over the rotating plate of an orbital shaker. Shaking was ceased during conductivity measurements. A home-made USP-type rotating disk apparatus made by Teflon and containing inside a magnetic stir bar was used for analysing sample S5: in this case the sample (about 100 mg) was pressed inside a cavity located on the disk surface and the disk was placed in a thermostatted beaker directly over a magnetic stirrer. Again stirring was interrupted during conductivity measurements.

Nuclear magnetic resonance (NMR). ^{1}H, ^{31}P, ^{23}Na, and ^{13}C NMR measurements were carried out through a Bruker Avance 300 MHz (7.05 T) spectrometer at the operating frequencies of 300.131, 121.495, 79.390, and 75.475 MHz respectively, at 25 °C. A standard variable temperature control unit (with an accuracy of 0.5 °C) was used.

Spin–lattice (T_1) and spin–spin (T_2) relaxation rates were obtained by means of the usual inversion recovery (180–τ–90–acquisition) and CPMG (90–τ–180–2τ–180–4τ–. . .–acquisition) acquisition sequences, respectively. The spin–lattice relaxation times, T_1, and the spin–spin relaxation times, T_2, were obtained by a three-parameter (for T_1, equation (A.1)) and by a two-parameter (for T_2, equation (A.2)) non-linear fit of the partially relaxed NMR signal intensities obtained at 14–18 different τ values.

$$I(\tau) = A - B\exp(-\tau/T_1) \tag{A.1}$$

$$I(\tau)_{\text{echo}} = C\exp(-\tau/T_2). \tag{A.2}$$

Self-diffusion coefficients were determined using a Bruker DIFF30 probe equipped with specific inserts for ^{1}H, ^{31}P, ^{23}Na, and ^{13}C nuclei and equipped by a Bruker Great 1/40 amplifier that can generate field gradients up to 1.2 T m^{-1}. The pulse-gradient stimulated echo (PGSTE) sequence was used and experiments were run varying the gradient strength (g) while keeping the gradient pulse length (δ) and the gradient pulse intervals (Δ) constant. Data were fitted to the modified Stejskal–Tanner equation for the PGSTE sequence [62, 63]:

$$I(g,\delta,\Delta,\tau_1,T) = I_0\exp\left[\left(-2\frac{\tau_1}{T_2}\right) - \left(\frac{\mathrm{T}}{T_1}\right)\right]\exp\left[-D\gamma^2 g^2\delta^2\left(\Delta - \frac{\delta}{3}\right)\right] \tag{A.3}$$

where I and I_0 are the echo intensity respectively in the presence and in the absence of the applied field gradient, γ is the gyromagnetic ratio of the investigated nucleus, τ_1 and T are the constant times between the first and the second and the second and the third 90° pulses and D is the self-diffusion coefficient. Self-diffusion coefficients were calculated by means of a two-parameter non-linear fit of the echo intensity decay measured at 14 different g values.

In particular, ^{1}H-decoupling was applied in all ^{13}C and ^{31}P NMR experiments.

In both relaxation times and self-diffusion NMR experiments the error on the fitting was always less than 1% (standard deviation). Errors in the NMR measurements are reported in terms of standard deviation on at least four different measurements.

Small-angle x-ray scattering. SAXS was recorded with a Kratky compact camera (HECUS MBraun, Graz, Austria). X-rays were generated by a Seifert ID-3003 x-ray generator, operating at 50 kV and 40 mA, equipped with a Cu-target sealed x-ray tube producing Cu Kα radiation with a wavelength of 1.542 Å. A 1D, position-sensitive wire-detector (OED 50M, MBraun, Garching, Germany) containing 1024 channels of width 54.0 mm was used for detection of scattered and diffracted x-rays in the small-angle region. The diffraction patterns were recorded at 25 °C. A PC-controlled Peltier element was used for temperature stabilization and control of

the sample. A few milligrams of the sample were enclosed in a stainless steel sample holder with Kapton windows. The distance between the sample and detector was 254 mm.

The lattice parameter (a) of the cubic phases was determined using the relation $d = 2\pi/q = \alpha/(h^2+k^2+l^2)^{1/2}$ from linear fits of the plots of q versus $(h^2+k^2+l^2)^{1/2}$, where q is the measured peak position and h, k, and l are the Miller indices.

Cryo-TEM. The experimental details have been reported elsewhere [13].

AFM. The experiments have been performed as reported in [15].

References

[1] Evans D F and Wennerstrom H 1994 *The Colloidal Domain: Where Physics, Chemistry, Biology, and Technology Meet* (New York: VCH)
[2] Jonsson B, Lindman B, Holmberg K and Kronberg B 1998 *Surfactants and Polymers in Aqueous Solution* (Chichester: Wiley)
[3] Ninham B W 1999 *Adv. Colloid Interface Sci.* **83** 1
[4] Malmsten M 2002 *Surfactants and Polymers in Drug Delivery* (New York: Dekker)
[5] Langer R 2001 *Science* **293** 58
[6] Langer R 2003 *Sci. Am.* **288** 50
[7] Kostarelos K 2003 *Adv. Colloid Interface Sci.* **106** 147
[8] Lee K Y and Mooney D J 2001 *Chem. Rev.* **101** 1869
[9] Bagwe R P, Kanicky J R, Palla B J, Patanjali P K and Shah D O 2001 *Crit. Rev. Ther. Drug Carrier Syst.* **18** 77
[10] Crommelin D J and Storm G 2003 *J. Liposome Res.* **13** 33
[11] Kabanov A V, Batrakova E V and Miller D W 2003 *Adv. Drug Deliv. Rev.* **55** 151
[12] Gustafsson J, Ljusberg-Wahren H, Almgren M and Larsson K 1996 *Langmuir* **12** 4611
[13] Gustafsson J, Ljusber-Wahren H, Almgren M and Larsson K 1997 *Langmuir* **13** 6964
[14] Landh T 1994 *J. Phys. Chem.* **98** 8453
[15] Neto C, Aloisi G, Baglioni P and Larsson K 1999 *J. Phys. Chem.* B **103** 3896
[16] Monduzzi M, Ljusberg-Wahren H and Larsson K 2000 *Langmuir* **16** 7355
[17] Nakano M, Sugita A, Matsuoka H and Handa T 2001 *Langmuir* **17** 3917
[18] Johnsson M, Barauskas J and Tiberg F 2005 *J. Am. Chem. Soc.* **127** 1076
[19] Tsiourvas D, Sideratou Z, Haralabakopoulos A A, Pistolis G and Paleos C M 1996 *J. Phys. Chem.* **100** 14087
[20] Marchi-Artzner V, Lehn J-M and Kunitake T 1998 *Langmuir* **14** 6470
[21] Berti D, Baglioni P, Bonaccio S, Barsacchi-Bo G and Luisi P L 1998 *J. Phys. Chem.* B **102** 303
[22] Berti D, Barbaro P, Bucci I and Baglioni P 1999 *J. Phys. Chem.* B **103** 4916
[23] Sideratou Z, Tsiourvas D, Paleos C M, Tsortos A, Pyrpassopoulos S and Nounesis G 2002 *Langmuir* **18** 829
[24] Sideratou Z, Foundis J, Tsiourvas D, Nezis I P, Papadimas G and Paleos C M 2002 *Langmuir* **18** 5036
[25] Baldelli-Bombelli F, Berti D, Keiderling U and Baglioni P 2002 *J. Phys. Chem.* B **106** 11613
[26] Verma S and Eckstein F 1998 *Annu. Rev. Biochem.* **67** 99
[27] Sihorkar V and Vyas S P 2001 *J. Pharm. Pharmaceut. Sci.* **4** 138
[28] Hyde S, Andersson S, Larsson K, Blum Z, Landh T, Lidin S and Ninham B W 1997 *The Language of Shape* (Amsterdam: Elsevier)
[29] Israelachvili J N, Mitchell D J and Ninham B W 1976 *J. Chem. Soc. Faraday Trans.* 2 **72** 1525
[30] Mitchell J D and Ninham B W 1981 *J. Chem. Soc. Faraday Trans.* 2 **77** 601
[31] Israelachvili J 1992 *Intermolecular and Surface Forces* 2nd edn (San Diego, CA: Academic)
[32] Andersson S, Hyde S T, Larsson K and Lidin S 1988 *Chem. Rev.* **88** 221
[33] Larsson K 1989 *J. Phys. Chem.* **93** 7304
[34] Hyde S T 1989 *J. Phys. Chem.* **93** 1458
[35] Larsson K 1967 *Z. Phys. Chem. Neue Folge* **56** 173
[36] Larsson K, Gabrielsson K and Lundberg B 1978 *J. Sci. Fd. Agric.* **29** 909
[37] Larsson K and Lindblom G 1982 *J. Disp. Sci. Technol.* **3** 61
[38] Larsson K 1983 *Nature* **304** 664
[39] Hyde S T, Andersson S, Ericsson B and Larsson K 1984 *Z. Kristallogr.* **168** 213
[40] Larsson K 1994 *Lipids—Molecular Organization, Physical Functions and Technical Applications* (Dundee: The Oily Press)
[41] Lawrence M J 1994 *Chem. Soc. Rev.* **23** 417
[42] Ganem-Quintanar A, Quintanar-Guerrero D and Buri P 2000 *Drug Develop. Ind. Pharm.* **26** 809

[43] Larsson K 2000 *Curr. Opin. Colloid Interface Sci.* **5** 64
[44] Mele S, Murgia S and Monduzzi M 2003 *Colloid. Surf.* A **228** 57
[45] Mele S, Murgia S, Caboi F and Monduzzi M 2004 *Langmuir* **20** 5241
[46] Caboi F, Nylander T, Razumas V, Talaikyté Z, Monduzzi M and Larsson K 1997 *Langmuir* **13** 5476
[47] Pitzalis P, Monduzzi M, Krög N, Larsson H, Ljusber-Wahren H and Nylander T 2000 *Langmuir* **16** 6358
[48] Caboi F, Amico G S, Pitzalis P, Monduzzi M, Nylander T and Larsson K 2001 *Chem. Phys. Lipids* **109** 47
[49] Murgia S, Caboi F and Monduzzi M 2001 *Chem. Phys. Lipids* **110** 11
[50] Murgia S, Caboi F, Monduzzi M, Ljusberg-Wahren H and Nylander T 2002 *Prog. Colloid Polym. Sci.* **120** 41
[51] Caboi F, Murgia S, Monduzzi M and Lazzari P 2002 *Langmuir* **18** 7916
[52] Caboi F, Nylander T and Monduzzi M 2003 *Report for Sardinia Region-Health Dept. Funds*
[53] Caboi F and Monduzzi M 1998 *Prog. Colloid Polym. Sci.* **108** 153
[54] Hyde S 1992 *Pure Appl. Chem.* **64** 1617
[55] Briggs J, Chung H and Caffrey M 1996 *J. Physique* II **6** 723
[56] Anderson D M and Wennerstrom H 1990 *J. Phys. Chem.* **94** 8683
[57] Razumas V, Kanapieniené J, Nylander T, Engström S and Larsson K 1994 *Anal. Chim. Acta* **289** 155
[58] Razumas V, Larsson K, Miezes Y and Nylander T 1996 *J. Phys. Chem.* **100** 11766
[59] Razumas V, Niaura G, Talaikyté Z, Vagonis A and Nylander T 2001 *Biophys. Chem.* **90** 75
[60] Eriksson P-O and Lindblom G 1993 *Biophys. J.* **64** 129
[61] Borné J, Nylander T and Khan A 2001 *Langmuir* **17** 7742
[62] Stejskal E O and Tanner J E 1965 *J. Chem. Phys.* **42** 288
[63] Stilbs P, Moseley M E and Lindman B 1980 *J. Magn. Reson.* **40** 401